

---

# Deeper Understanding of Black-box Predictions via Generalized Influence Functions

---

Hyeonsu Lyu Jonggyu Jang Sehyun Ryu Hyun Jong Yang  
POSTECH, Korea  
{hslyu4, jgjang, sh.ryu, hyunyang}@postech.ac.kr

## Abstract

Influence functions (IFs) elucidate how training data changes model behavior. However, the increasing size and non-convexity in large-scale models make IFs inaccurate. We suspect that the fragility comes from the first-order approximation which may cause nuisance changes in parameters irrelevant to the examined data. However, simply computing influence from the chosen parameters can be misleading, as it fails to nullify the hidden effects of unselected parameters on the analyzed data. Thus, our approach introduces generalized IFs, precisely estimating target parameters' influence while nullifying nuisance gradient changes on fixed parameters. We identify target update parameters closely associated with the input data by the output- and gradient-based parameter selection methods. We verify the generalized IFs with various alternatives of IFs on the class removal and label change tasks. The experiments align with the "less is more" philosophy, demonstrating that updating only 5% of the model produces more accurate results than other influence functions across all tasks. We believe our proposal works as a foundational tool for optimizing models, conducting data analysis, and enhancing AI interpretability beyond the limitation of IFs.

## 1 Introduction

The quote "*Fear always springs from ignorance* – Emerson (1841)" well represents the anxiety of our society on AI. The requests from worldwide scholars and entrepreneurs to stop developing large language models reflect such growing concern (Anderson, 2023). Technological advancements over a couple of decades have shown the astonishing capabilities of AI, yet the extent to which AI can expand remains unknown.

Influence functions, originating from classical statistics (Hampel, 1974), have appeared as a breakthrough to address societal concerns. Influence functions provide explainability and accessibility to the enigmatic black-box models by measuring how the model changes when some training examples are deleted or perturbed (Koh & Liang, 2017; Barredo Arrieta et al., 2020). Diverse tasks are proposed and resolved in the realm of influence functions, including data preprocessing (Lee et al., 2020; Yang et al., 2023), natural language processing (Jain et al., 2022; Ye et al., 2022), post-hoc processing (Kong et al., 2022), and model attacks (Cohen & Giryes, 2022; Koh et al., 2022). However, their deficiencies have been consistently reported when applied to large-scale models or large data groups.

Koh et al. (2019); Basu et al. (2020b) revealed that influence functions become increasingly inaccurate for large data groups, as the estimation error scales quadratically with the size of the removed data. Concurrently, Basu et al. (2021) observed found that an increase in the parameter count correlates with reduced accuracy of influence functions. However, there are no thorough explanations for why the number of parameters affects the accuracy to the best of our knowledge.

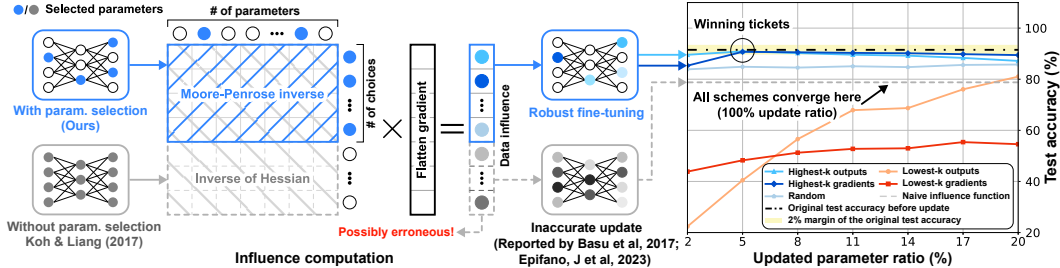


Figure 1: Overview of our approach and the original influence functions with the test accuracy per updated parameter ratio for various parameter selection schemes. Both Koh & Liang (2017) and our approach linearly transform the gradient of examined data, but our method negates changes in irrelevant parameters by projecting the gradient into the space of selected parameters.

A suspicious candidate is the estimation error. Influence functions adopt first-order Taylor approximation to measure the change of the *entire* parameters. However, not all parameters are involved with a given input data (Olah et al., 2018; Bau et al., 2020), so nuisance changes from approximation errors could accumulate in the irrelevant parameters and cause lossy updates. This hypothesis explains why influence functions become inaccurate as the network size increases. Metaphorically speaking, conducting network-wide sweeps through influence functions could be similar to removing a brain segment to treat an ankle sprain.

**Our approach.** We verify our conjecture by proposing a generalized influence function (GIF), which measures the model changes only in the parameters closely associated with the input data. We establish parameter selection criteria to efficiently distinguish between relevant and irrelevant parameters during feed-forward and back-propagation, inspired by the lottery-ticket hypothesis of the network pruning (Frankle & Carbin, 2019; Wang et al., 2020). Figure 1 illustrates how the GIF computes the data influence compared to the original influence functions. We confirm that using irrelevant parameters can harm model performance, and identify winning tickets that closely maintain the original model’s capabilities.

We also find a remarkable property of the GIF, which makes the LiSSA algorithm, a fast approximation of influence functions, to *always converge in any network*, maintaining the complexity as linear. The LiSSA algorithm is the key method to compute influence functions within feasible cost (Agarwal et al., 2017; Koh & Liang, 2017). However, the algorithm frequently diverges if the model is non-convex (Basu et al., 2021; Epifano et al., 2023), enforcing the loss function to have a  $L_2$  regularization (Koh et al., 2019; Grosse et al., 2023).<sup>1</sup>

Benchmarks with the five contemporary methods in small-scale models show that the GIFs can provide more accurate inference results in the class removal and label change tasks. Remarkably, updating only 5% parameters via GIF can tightly maintain the test accuracy of the original model while almost perfectly deleting or changing a large portion of data. Inference-time analysis including model distributions and discriminative region visualization (Selvaraju et al., 2017) reveals that updating only a small portion of parameters can robustly replicate the behavior of a network retrained from scratch without the removed data points.

## 2 Preliminaries: What is Influence Function?

**Notations and definitions.** The remainder of the paper shares the following definitions and notations for consistency. We consider a model  $\theta$  of size  $n$  in the parameter space  $\Theta \subset \mathbb{R}^n$  and  $m$  training examples  $z_1, \dots, z_m \in Z$ .

An empirical risk is defined as  $\mathcal{L}(\theta) = \frac{1}{m} \sum_{i=1}^m \ell(z_i, \theta)$  for some loss function  $\ell(\cdot)$ . The empirical risk minimizer  $\hat{\theta}$  is accordingly defined as  $\hat{\theta} = \operatorname{argmin}_{\theta \in \Theta} \mathcal{L}(\theta)$ . Additionally, An  $\epsilon$ -upweighted empirical risk minimizer is defined as

$$\hat{\theta}(\epsilon, \mathbf{w}) = \operatorname{argmin}_{\theta \in \Theta} \mathcal{L}(\theta) + \epsilon \sum_{i=1}^m w_i \ell(z_i, \theta), \quad (1)$$

<sup>1</sup> $L_2$  regularization with weight  $\lambda$  makes loss functions convex by shifting the eigenvalue of Hessian by  $\lambda$ .

where  $\mathbf{w} = [w_1, \dots, w_m]^\top \in \{0, 1\}^m$  indicates whether each training example is upweighted or not. The influence of a single data point can be measured by setting  $\mathbf{w}$  as a one-hot vector.

**Original influence function.** Koh & Liang (2017) introduced an influence function, which measures the parameter change when the empirical risk changes infinitesimally for given data. The influence function  $\mathcal{I}(\mathbf{w}, \hat{\boldsymbol{\theta}})$  computes the change direction from  $\hat{\boldsymbol{\theta}}$  to  $\hat{\boldsymbol{\theta}}(\epsilon, \mathbf{w})$ .

Influence functions can be derived as follows (see, e.g., Koh & Liang (2017) for details). By applying Taylor expansion with  $\hat{\boldsymbol{\theta}}$  as an anchor, the first-order optimality condition of the  $\epsilon$ -upweight risk at  $\hat{\boldsymbol{\theta}}(\epsilon, \mathbf{w})$  can be linearly approximated as

$$0 \approx \epsilon \sum_{i=1}^m w_i \nabla \ell(z_i, \hat{\boldsymbol{\theta}}) + \mathbf{H}(\hat{\boldsymbol{\theta}}(\epsilon, \mathbf{w}) - \hat{\boldsymbol{\theta}}) \iff \hat{\boldsymbol{\theta}}(\epsilon, \mathbf{w}) - \hat{\boldsymbol{\theta}} \approx -\mathbf{H}^{-1} \left[ \sum_{i=1}^m w_i \nabla \ell(z_i, \hat{\boldsymbol{\theta}}) \right] \epsilon, \quad (2)$$

where Hessian  $\mathbf{H}$  is equal to  $[\mathbf{h}_1 | \dots | \mathbf{h}_n] = \sum_{i=1}^m (1 + \epsilon w_i) \nabla^2 \ell(z_i, \hat{\boldsymbol{\theta}}) \in \mathbb{R}^{n \times n}$ . From (2), influence function can be defined as

$$\mathcal{I}(\mathbf{w}, \hat{\boldsymbol{\theta}}) := \left. \frac{d(\hat{\boldsymbol{\theta}}(\epsilon, \mathbf{w}) - \hat{\boldsymbol{\theta}})}{d\epsilon} \right|_{\epsilon=0} = -\mathbf{H}^{-1} \left[ \sum_{i=1}^m w_i \nabla \ell(z_i, \hat{\boldsymbol{\theta}}) \right]. \quad (3)$$

**LiSSA iteration: fast influence approximation** Koh & Liang (2017); Basu et al. (2020b) propose an iterative method that can approximately compute inverse-Hessian-vector product by using the Neuman series (Stewart, 2001), Hessian-vector product (Pearlmutter, 1994), and the LiSSA algorithm (Agarwal et al., 2017). The iterative approximation can be represented as

$$\mathcal{I}_k = \mathcal{I}_0 + (\mathbf{I} - \mathbf{H}_{\hat{\boldsymbol{\theta}}}) \mathcal{I}_{k-1}, \quad (4)$$

where  $\mathcal{I}_0 = \nabla \ell(z, \hat{\boldsymbol{\theta}})$  and  $\mathbf{H}_{\hat{\boldsymbol{\theta}}}$  is estimated from uniformly chosen  $t$  data samples  $z_{s_1}, \dots, z_{s_t}$ .

This recursive series converges as  $\mathcal{I}_k \rightarrow \mathcal{I}(z, \hat{\boldsymbol{\theta}})$  as  $k \rightarrow \infty$  only if  $\rho(\mathbf{I} - \mathbf{H}_{\hat{\boldsymbol{\theta}}}) < 1$  for spectral radius  $\rho(\cdot)$ .<sup>2</sup> In other words, all eigenvalues of the estimated Hessian must be within  $[0, 2)$ , which is hardly the case. Thus, Koh et al. (2019); Basu et al. (2020b) apply  $L_2$ -regularization and scale the loss down to avoid the divergence of the series. Nonetheless,  $L_2$ -regularization is not a silver bullet for the convergence of the series (4) because there is no way to pre-determine proper regularization weight to make the empirical risk convex for a given model (Appendix A).

## 2.1 Popular Usage Cases

**Data removal (G. Wu et al. 2022; J. Wu et al. 2023).** Taking  $\epsilon = -1/m$  can remove the influence of data  $z_i$  corresponding to  $w_i = 1$  from the model as  $\epsilon = -1/m$  cancels  $\ell(z_i, \hat{\boldsymbol{\theta}})$  from upweighted the empirical risk (1). That is, we can approximate  $\hat{\boldsymbol{\theta}}(\epsilon, \mathbf{w})$  by updating the parameter as  $\hat{\boldsymbol{\theta}} \leftarrow \hat{\boldsymbol{\theta}} - \frac{1}{m} \mathcal{I}(\mathbf{w}, \hat{\boldsymbol{\theta}})$  according to (2).

**Data perturbation (Kong et al., 2022; Gong et al., 2022; Lee et al., 2020).** Influence functions can measure the approximated parameter changes from  $\hat{\boldsymbol{\theta}}$  to the model retrained with  $Z'$  when the training dataset changes from  $Z$  to  $Z'$ . Suppose that binary vector  $\mathbf{w} \in \mathbb{R}^m$  indicates  $w_i = 1$  if  $z_i \neq z'_i$  for  $z_i \in Z, z'_i \in Z'$ , otherwise  $w_i = 0$ . Then, another influence function  $\mathcal{I}_{Z'}(\mathbf{w}, \hat{\boldsymbol{\theta}}) = -\mathbf{H}^{-1} \left[ \sum_{i=1}^m w_i \nabla \ell(z'_i, \hat{\boldsymbol{\theta}}) \right]$  can be defined. Similar to **Data removal**, the parameter can be updated as  $\hat{\boldsymbol{\theta}} \leftarrow \hat{\boldsymbol{\theta}} - \frac{1}{m} \mathcal{I}(\mathbf{w}, \hat{\boldsymbol{\theta}}) + \frac{1}{m} \mathcal{I}_{Z'}(\mathbf{w}, \hat{\boldsymbol{\theta}})$  (Koh & Liang, 2017).

**Data scoring (Yang et al., 2023; Schioppa et al., 2022; Guo et al., 2021).** The influence of data for given  $\mathbf{w}$  on the test data  $z_{\text{test}}$  is defined as  $\mathcal{I}(z_{\text{test}}, \mathbf{w}, \hat{\boldsymbol{\theta}}) = \langle \nabla \ell(z, \hat{\boldsymbol{\theta}}), \mathcal{I}(\mathbf{w}, \hat{\boldsymbol{\theta}}) \rangle$  (Koh & Liang, 2017). This metric is adopted by widespread applications including data sampling, data influence scoring, and mislabel detection tasks.

<sup>2</sup>The spectral radius of matrix  $\mathbf{A} \in \mathbb{R}^{n \times n}$  is defined as  $\rho(\mathbf{A}) = \max\{|\lambda_1|, \dots, |\lambda_n|\}$ , where  $\lambda_1, \dots, \lambda_n$  are the eigenvalues of  $\mathbf{A}$ .

### 3 Proposed Method: Generalized Influence Function

The driving questions behind our approach are:

*How can we measure the influence of data only for the selected relevant parameters?  
How can we nullify changes in irrelevant parameters?*

Unfortunately, the original influence function (3) cannot be an answer as it can only measure the holistic model changes. We instead answer the question by separating parameters into i) **target parameters** for measuring the influence, and ii) **fixed parameters** to be unchanged.

Fig. 2 indicates that the original influence function fails to minimize the mean-square error of the  $\mathbb{R}^6 \mapsto \mathbb{R}$  linear regression problem in the data removal task. The influence of  $(\theta_1, \theta_2)$  can be measured by **freezing** the unselected parameters or naively **projecting** the original influence function with the indices of selected parameters. However, these methods overlook the subliminal effect of the fixed parameters, resulting in erroneous updates. In-depth explanations about the freezing and projecting are provided in Sec. 5 and Appendix B.

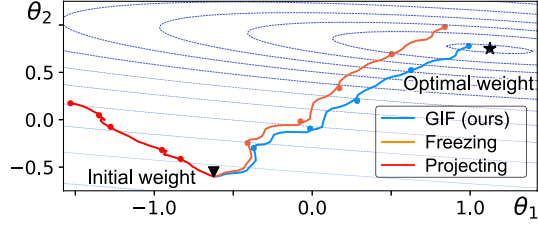


Figure 2: Visualization of the weight updates via three influence functions. The contour represents the level curve of the loss. The circular markers represent every 10th removal of four data points. The optimal weight indicates  $(\theta_1, \theta_2)$  that provides the least loss when freezing the other parameters.

**Definition.** Let us denote each element of parameter  $\theta$  as  $\theta_1, \dots, \theta_n$  where  $\theta = [\theta_1, \dots, \theta_n]^\top$ . By using the index set  $J = \{j_1, \dots, j_k\}$  with  $k$  indices, we define a sub-parameter  $\theta_J = [\theta_{j_1}, \dots, \theta_{j_k}]^\top \in \mathbb{R}^k$  and  $\theta_{-J} = [\theta_j]_{j \notin J} \in \mathbb{R}^{n-k}$ , which indicate the target parameters and fixed parameters, respectively. For brevity, we rearrange all terms in (2) as  $\hat{\theta} = [\hat{\theta}_J, \hat{\theta}_{-J}]^\top$  and  $\mathbf{H} = [\mathbf{H}_J | \mathbf{H}_{-J}]$  for  $\mathbf{H}_J = [\mathbf{h}_j]_{j \in J}$  and  $\mathbf{H}_{-J} = [\mathbf{h}_i]_{i \notin J}$ .

We assume that parameters in  $J$  are stationary, which implies that the model changes from  $\hat{\theta} = [\hat{\theta}_J, \hat{\theta}_{-J}]^\top$  to  $\hat{\theta}(\epsilon, \mathbf{w}) = [\hat{\theta}_J(\epsilon, \mathbf{w}), \hat{\theta}_{-J}]^\top$ . Then, (2) is represented as

$$0 \approx \epsilon \sum_{i=1}^m w_i \nabla \ell(z, \hat{\theta}) + [\mathbf{H}_J | \mathbf{H}_{-J}] \left( \begin{bmatrix} \hat{\theta}_J(\epsilon, \mathbf{w}) \\ \hat{\theta}_{-J} \end{bmatrix} - \begin{bmatrix} \hat{\theta}_J \\ \hat{\theta}_{-J} \end{bmatrix} \right) = \epsilon \nabla \ell(z, \hat{\theta}) + \mathbf{H}_J \Delta_\epsilon, \quad (5)$$

for  $\Delta_\epsilon = \hat{\theta}_J(\epsilon, \mathbf{w}) - \hat{\theta}_J \in \mathbb{R}^k$  as the  $\hat{\theta}_{-J}$  terms cancel each other, not affecting the equation.

Finding  $\Delta_\epsilon$  in (5) is an overdetermined problem where the Moore-Penrose inverse provides mathematical optimum as in the case of the least-square method (Ben-Israel & Greville, 2003). Then, the influence of data point  $z$  on  $\hat{\theta}_J$  is defined as (See Appendix C for a detailed derivation)

$$\mathcal{I}(\mathbf{w}, \hat{\theta}_J | \hat{\theta}) = \frac{d\Delta_\epsilon}{d\epsilon} = (\mathbf{H}_J^\top \mathbf{H}_J)^{-1} \mathbf{H}_J^\top \left[ \sum_{i=1}^m w_i \nabla \ell(z_i, \hat{\theta}) \right], \quad (6)$$

**Special case.** The original influence function (3) can be reproduced from (6) by setting  $\hat{\theta}_J = \hat{\theta}$  with  $J = \{1, \dots, n\}$ . Then, sub-matrix  $\mathbf{H}_J = \mathbf{H}$  becomes full-rank, which corresponds to

$$\mathcal{I}(z, \hat{\theta} | \hat{\theta}) = -\mathbf{H}^{-1} \nabla \ell(z, \hat{\theta}) = \mathcal{I}(z, \hat{\theta}). \quad (7)$$

**Upweight effect in data removal.** The  $\epsilon$  term could have a substantial effect when the proportion of the upweighted data is large (Koh et al., 2019; Basu et al., 2020b), though the effect is negligible when calculating the influence of an individual data point (Koh & Liang, 2017). For example, when we take  $\epsilon = -\frac{1}{m}$  to remove data group from the model, then Hessian  $\mathbf{H}|_{\epsilon=-1/m} = \frac{1}{m} \sum_{i=1}^m (1-w_i) \nabla^2 \ell(z_i, \hat{\theta})$  excludes the loss from upweighted data.<sup>3</sup> This aligns with the observation by Koh et al. (2019), indicating that  $\mathbf{H}|_{\epsilon=-1/m}$ , referred to as Newton approximation, provides a more accurate estimation compared to the Hessian of original influence function  $\mathbf{H}|_{\epsilon=0}$ .

<sup>3</sup>We omit the notation of  $\epsilon$  in  $\mathbf{H}_J$  and  $\mathbf{H}$  for the brevity of notations.

### 3.1 Modified LiSSA: Toward Fast and Guaranteed Convergence

**Definition.** We tailor a modified LiSSA which does not require any specific loss function, especially  $L_2$  regularization. The series (4) can be extended to the case of GIF as

$$\mathcal{I}_k = \mathcal{I}_0 + (\mathbf{I} - \mathbf{H}_J^\top \mathbf{H}_J) \mathcal{I}_{k-1}, \quad \mathcal{I}_0 = \mathbf{H}_J^\top \left[ \sum_{i=1}^m w_i \nabla \ell(z_i, \hat{\boldsymbol{\theta}}) \right]. \quad (8)$$

Then, the series converges to the GIF  $\mathcal{I}(z, \hat{\boldsymbol{\theta}}_J | \hat{\boldsymbol{\theta}})$  as  $k \rightarrow \infty$  only if  $\rho(\mathbf{I} - \mathbf{H}_J^\top \mathbf{H}_J) < 1$ . As in (7), taking  $J$  as full parameter index  $J = \{1, \dots, n\}$  makes the above series converge to the original influence function (3). Appendix A describes detailed derivations.

**Guaranteed convergence.** We find a simple, straightforward method to guarantee the iteration converging. Certainly, the series itself might diverge, yet the proposition below ensures that there is always a loss and empirical risk towards which the series (8) converges stably.

**Proposition 3.1.** *For any  $\ell(\cdot)$  and  $\mathcal{L}(\cdot)$ , the following statements hold:*

- i) *The GIF is scale-invariant. That is, scalar multiplication on the loss  $\ell(\cdot)$  and empirical risk  $\mathcal{L}(\cdot)$  does not change  $\mathcal{I}(\mathbf{w}, \hat{\boldsymbol{\theta}}_J | \hat{\boldsymbol{\theta}})$ .*
- ii) *There always exists  $M > 0$  that makes the series (8) for the scaled loss  $\frac{1}{M} \ell(\cdot)$  and empirical risk  $\frac{1}{M} \mathcal{L}(\cdot)$  converge.*

*Proof.* See Appendix E. □

There is a convenient strategy to find proper  $M$  instead of theoretically determining  $M$ . We just execute the modified LiSSA iteration (8). If the series diverges, we restart the iteration after dividing the loss  $\ell(\cdot)$  and empirical risk  $\mathcal{L}(\cdot)$  by some decaying factor  $M$ . This strategy is widespread in the field of second-order optimization such as the Levenberg-Marquardt algorithm (Transtrum et al., 2011) and the backtracking line-search technique (Bertsekas, 2016).

We can avoid the direct  $\mathcal{O}(n^3)$  computation of  $\mathbf{H}_J^\top \mathbf{H}_J$  by cleverly applying HVP. Note that  $\mathbf{H}_J^\top \mathbf{H}_J$  is the  $k \times k$  leading principal submatrix of  $\mathbf{H}^\top \mathbf{H}$ , so the following equality holds for any  $v \in \mathbb{R}^k$ :

$$\mathbf{H}^\top \mathbf{H} \begin{bmatrix} v \\ \mathbf{0} \end{bmatrix} = \begin{bmatrix} \mathbf{H}_J^\top \\ \mathbf{H}_{-J}^\top \end{bmatrix} [\mathbf{H}_J | \mathbf{H}_{-J}] \begin{bmatrix} v \\ \mathbf{0} \end{bmatrix} = \begin{bmatrix} \mathbf{H}_J^\top \mathbf{H}_J v \\ \mathbf{H}_J^\top \mathbf{H}_{-J} v \end{bmatrix}. \quad (9)$$

Therefore, the series in Prop. 3.1 can be computed by applying the HVP twice, which takes the same complexity  $\mathcal{O}(n)$  as the original IF.

## 4 Identifying Suitable Target Parameters

Which parameters should we modify to remove or change trained data points? The primary goal of the GIF is to precisely estimate significant changes in model behavior when multiple data points are deleted or changed from the model. To do so, classifying highly relevant parameter  $\boldsymbol{\theta}_J$  is crucial, as we guess that nuisance changes from influence functions might accumulate in irrelevant parameters. Unfortunately, computing the GIF for every possible  $J$  is infeasible even for a simple network. The number of combinations for choosing 100 parameters out of 1000 parameters ( $\approx 10^{140}$ ) outstrips the number of atoms in the universe ( $\approx 10^{82}$ ).

We propose empirical parameter selection methods to detour the combinatorial explosion, inspired by the neurological approach that analyzes how the specific areas of the brain respond to certain tasks or stimuli (Penny et al., 2011). We are also motivated by network pruning and quantization, which remove the least important connections to compress the network Hu et al. (2016); Lee et al. (2019).

**Parameter selection criteria.** We design two criteria, so-called **Highest- $k$  outputs** and **Highest- $k$  gradients** that select  $k\%$  of parameters that produce the highest outputs and gradients for input data, respectively. Layer outputs from parameters irrelevant to input data might be filtered out by the activation functions, so the corresponding outputs and gradients become negligible. Conversely, we assume that these selection criteria can select valid parameters for a given data input.

These criteria are compared with the **Lowest- $k$  outputs** and **Lowest- $k$  gradients**, which pick  $k\%$  of parameters that generate the lowest outputs and gradients, respectively; and **Random** that uniformly selects  $k\%$  of parameters.

The number of selected parameters  $k$  is determined proportional to the number of parameters for each layer. Without having an additional selection process, these methods can be implemented as callback functions that are executed when each layer is processed during the feed-forward or back-propagation.

The GIF algorithm can be devised by combining the numerical series (8) and the parameter selection method, as in Alg. 1. The GIF for a single data point can be computed by defining the indicator vector  $w$  as a one-hot vector. Once  $\mathcal{L}(\hat{\theta})$ ,  $\mathcal{L}_w(\hat{\theta})$  and  $J$  are given, the series (8) can be computed by using the hessian vector-product.

---

#### Algorithm 1 Generalized Influence Function

---

- 1: **Input:**  $\hat{\theta}$ ,  $w \in \{1, 0\}^m$ ,  $k = 1, k_{\max}, \mu$ .
  - 2:  $\mathcal{L}(\hat{\theta}) \leftarrow \sum_{i=1}^m \ell(z_i, \hat{\theta})$ ,  $\mathcal{L}_w(\hat{\theta}) \leftarrow \sum_{i=1}^m w_i \ell(z_i, \hat{\theta})$ .
  - 3: Determine  $J$  using one of the selection criteria.
  - 4: **repeat**
  - 5:  $\mathcal{I}_k \leftarrow \mathcal{I}_0 + (\mathbf{I} - \mathbf{H}_J^T \mathbf{H}_J) \mathcal{I}_{k-1}$  # By using (9).
  - 6: **if**  $\mathcal{I}_k$  is diverging, **then**
  - 7:  $\mathcal{L}(\hat{\theta}) \leftarrow \mathcal{L}(\hat{\theta})/\mu$ ,  $\mathcal{L}_w(\hat{\theta}) \leftarrow \mathcal{L}_w(\hat{\theta})/\mu$ .
  - 8: Restart the loop from scratch with  $k \leftarrow 1$ .
  - 9: **end if**
  - 10:  $k \leftarrow k + 1$ .
  - 11: **until**  $\|\mathcal{I}_k - \mathcal{I}_{k-1}\| \geq \epsilon$  or  $k \neq k_{\max}$ .
- 

\* Pythonic pseudo-code is provided in Appendix F.

## 5 Findings Through Experiments

Inspired by Koh et al. (2019), we evaluate the GIF in the data removal and label change tasks by the below metrics to check whether the updated model genuinely tracks the model retrained from scratch. We update the model as described in Sec. 2.1. A detailed explanation of the update is also provided in Appendix G.3.

- **Test loss:** The loss on the test dataset  $Z_{\text{test}}$ , denoted as  $\sum_{z \in Z_{\text{test}}} \ell(z, \hat{\theta})$ , measures the effect of removing or changing a data subset on the test prediction.
- **Test accuracy:** The accuracy on the test dataset  $Z_{\text{test}}$ , similar to the test loss.
- **Self-loss:** The loss of the removed data, denoted as  $\sum_{i=1}^m w_i \ell(z_i, \hat{\theta})$ . Comparison with the model retrained without  $z_i \in Z$  for  $w_i = 1$  provides how accurately the model is updated.
- **self-accuracy:** The accuracy on the removed data, akin to the self-loss.

We conduct all experiments at NVIDIA Geforce RTX 3080Ti with 12GB VRAM.

### 5.1 Lottery Ticket Hypothesis in Influence Functions

We have proposed a conjecture that erroneous updates in the irrelevant parameters may degrade the model performance. The five selection criteria above are evaluated on the VGG-11 network trained with the CIFAR-10 dataset to verify the guess. We first measure the influence of images labeled as "0" by Alg. 1, then remove the trained images by repetitively adding the influence to the model with update rate  $\gamma = 0.06$  until the self-accuracy becomes lower than 0.4%.

**Results.** Figure 3 illustrates that two **Highest- $k$**  criteria outperform the baselines, which verifies the existence of winning tickets in the parameter combination as in the case of network pruning (Frankle & Carbin, 2019). **Highest- $k$  outputs** and **gradients** show 91.47% and 91.50% test accuracies with the 91.50% of original test-accuracy.

Also, two **Lowest- $k$  criteria** imply that the fragility of the influence function comes from the excessive modifications of irrelevant parameters. Then,

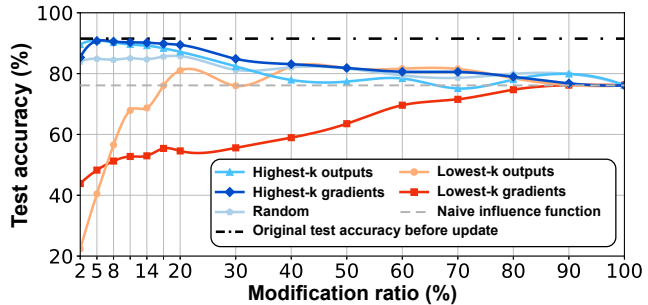


Figure 3: Test accuracy evaluation for various parameter selection criteria. The modification ratio indicates the ratio of parameters updated.

**naive influence functions** (Koh & Liang, 2017) provide inferior accuracy (76.13%) compared to the accuracy of **Random** criteria (75-85%).

## 5.2 Performance Evaluation on Class Removal Task

We evaluate the losses and accuracies of the GIF, extending the linear regression with synthetic data points in Fig. 2. We conduct a class removal task on the VGG-11 with the CIFAR-10 dataset and remove training points labeled as "8". The GIF is compared with the following baselines:

- **Freezing, inspired by Guo et al. (2021)**: One viable approach involves the selective freezing of parameters  $\theta_j$ ,  $j \notin J$ , computing the influence through (2). This approach is reminiscent of layer-wise freezing approaches in Koh & Liang (2017) and Guo et al. (2021).
- **Projecting, inspired by Schioppa et al. (2022)**: Influence functions for chosen parameters can also be computed by extracting indices in  $J$  from the influence (7). This process is equivalent to the naive projection from the original space to parameter space  $\hat{\theta}_J$ .
- **Original (Koh & Liang, 2017)**: The original influence functions introduced in Sec. 2.
- **Second-order (Basu et al., 2020a)**: The method adopts second-order approximation of model changes to improve correlations between the estimated and actual changes, whereas ordinary influence functions utilize linear approximation.
- **Few-shot unlearning (Yoon et al., 2023)**: This method removes unwanted influences of training data by using the scrubbing procedure, which randomly changes the labels of target data and relearns the network from the early checkpoint.<sup>4</sup>

Table 1: Benchmarks of influence functions in the data removal task. Test {accuracies and losses} are evaluated on the CIFAR-10 test dataset, excluding data points labeled with "8". Desirable model behavior after fine-tuning should emulate the model trained from scratch without target removal data, marked as up and down arrows. The **best** is marked as bold blue.

Methods	MR%	Test acc. (%) $\uparrow$	Test loss $\downarrow$	Self-acc. (%) $\downarrow$	Self-loss $\uparrow$	$F_1$ score $\uparrow$
Before update	-	91.07	0.38	93.80	0.27	-
<b>GIF (ours)</b>	5%	<b>90.13<math>\pm</math>1.60</b>	<b>0.42<math>\pm</math>0.09</b>	<b>0.26<math>\pm</math>0.65</b>	5.31 $\pm$ 1.2352	<b>0.9469</b>
	15%	89.31 $\pm$ 1.73	0.44 $\pm$ 0.10	0.56 $\pm$ 0.82	6.70 $\pm$ 1.2712	0.9410
	30%	87.93 $\pm$ 1.50	0.49 $\pm$ 0.10	0.76 $\pm$ 0.87	8.04 $\pm$ 0.8816	0.9324
Freezing (Guo et al., 2021)	5%	89.24 $\pm$ 2.11	0.45 $\pm$ 0.12	0.41 $\pm$ 0.80	5.93 $\pm$ 1.4936	0.9412
	15%	88.78 $\pm$ 2.10	0.46 $\pm$ 0.13	0.45 $\pm$ 0.91	6.99 $\pm$ 1.6772	0.9385
	30%	88.42 $\pm$ 1.89	0.47 $\pm$ 0.12	0.63 $\pm$ 0.80	7.67 $\pm$ 1.2774	0.9357
Projecting (Schioppa et al., 2022)	5%	87.95 $\pm$ 2.65	0.52 $\pm$ 0.16	0.72 $\pm$ 0.77	7.49 $\pm$ 0.9617	0.9326
	15%	87.27 $\pm$ 1.84	0.54 $\pm$ 0.12	1.41 $\pm$ 1.48	7.99 $\pm$ 0.8038	0.9258
	30%	86.89 $\pm$ 1.95	0.55 $\pm$ 0.13	1.31 $\pm$ 0.98	8.16 $\pm$ 0.8984	0.9241
Koh & Liang (2017)	100%	86.06 $\pm$ 2.17	0.60 $\pm$ 0.14	1.29 $\pm$ 0.68	<b>8.66<math>\pm</math>1.0469</b>	0.9194
Basu et al. (2020a)	100%	84.34 $\pm$ 1.90	0.71 $\pm$ 0.11	2.63 $\pm$ 1.20	7.97 $\pm$ 0.5917	0.9038
Yoon et al. (2023)	-	86.4 $\pm$ 0.7	-	1.6 $\pm$ 1.0	-	0.9201
From-scratch retraining	-	91.79	0.34	0.00	8.66	0.9572

**Results.** Table 1 shows the evaluation results from a handful of the IF schemes and the unlearning scheme. The GIF scheme outperforms the other two methods for the {self, test}-accuracy and test loss. Especially when the modification ratio (MR) is 5%, the **GIF** well eradicates the trained data from the network, closely approximating the retrained network. The closest model to the retraining is obtained by the **GIF** with MR@5%, showing **91.51%** and **0.00%** of the {test, self} accuracies, respectively. The **Projecting** scheme at MR@5% provides better self-accuracy and loss, but the test accuracy and loss are significantly sacrificed while the **GIF** well preserves the network utility. The **Original** and **second-order**, full parameter update schemes, show lower performance than the partial

<sup>4</sup>We directly refer to the experimental result as we cannot access the experimental code and network architecture. We keep all experimental setups consistent except for the network structure.

parameter update schemes. These results align with our observation in Fig. 3. Also, the **Few-shot unlearning** provides lower performance than the **GIF** as the scrubbing process contaminates the training dataset by randomly changing labels of target removal data.

### 5.3 Performance Evaluation Against Backdoor Attack Scenario

We further verify the GIF in a backdoor (BD) recovery scenario to ensure that the proposed scheme genuinely modifies the network, not manipulating the results. The results from the data removal task could be fabricated as we can make a softmax output zero by allocating a large negative value to the associated bias.

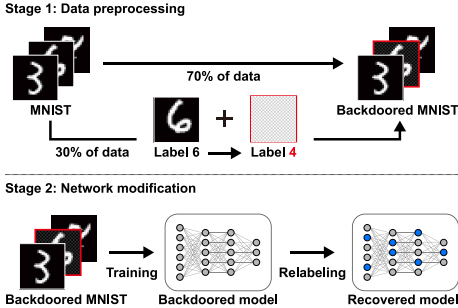


Figure 4: Backdoor recovery scenario.

As illustrated in Fig. 4, the BD dataset is generated by implanting the backdoor pattern on randomly chosen data and changing the label as a backdoor label in Stage 1. Then, the model trained with the BD dataset returns a BD label for given BD data, but it normally operates for normal input data. At Stage 2, if the influence functions properly recover the model, the model should generate proper outputs for both BD and non-BD data. A canonical neural network is utilized as a BD model, which consists of four convolutional layers and one fully connected layer.

**Results.** Table 2 lists the accuracy of the models in the BD scenario. The **GIF**, **Freezing**, and **Projecting** schemes are evaluated with 5% MR as they provide the best results. The **GIF** successfully recovers the original model by just conducting one-shot modification on 5% of parameters, showing that the GIF recognizes and properly modifies parameters associated with the backdoor patterns. The **Projecting** achieves a comparable accuracy to the **GIF** for BD data with the BD label; but records lower accuracies for test data and BD data with the original label. Also, the **Original** and **Second-order** show similar accuracy for the test dataset compared to the **GIF**, but underperform on the BD recovery task.

### 5.4 Will the GIF Genuinely Update Model like From-Scratch Retrained Model?

The GIF only updates a small model segment, leaving most parameters equal to the parameters from the original model. However, this might contradict the nature of influence functions that make the updated model behave similarly to the model retrained from scratch with the changed dataset. Tables 1 and 2 indirectly show that the GIF closely follows the behavior of the **Retraining** compared to the other baselines. In addition, we further verify how the updated model internally behaves by observing output distributions and Gradient-weighted Class Activation Mapping (Grad-CAM) visualization (Selvaraju et al., 2017) of the updated model.

**Inference histogram.** We first train the VGG-11 network (**before**) with the CIFAR-10 dataset, then conduct a data removal task using the GIF. The **Highest- $k$  gradients** selects 5, 15, 30% of model parameters. The selected parameters are then updated via the GIF, denoted as **MR@{5, 15, 30}%**, respectively. Lastly, we retrain the network from scratch (**retraining**) excluding the target removal data. Figure 5 shows how often each label is inferred when deleted data is provided on each network. Remarkably, the histogram obtained from **MR@{5, 15, 30}%** shows a similar tendency with the **retraining**, showing the robustness of the partial parameter update.

Table 2: Accuracies of models recovered by various influence functions. The **best** is marked as bold blue.

Method	Test dataset	BD data w/ true label	BD data w/ BD label
BD Model	99.61	9.42	100.00
<b>GIF (ours)</b>	<b>98.26 ± 0.66</b>	<b>95.38 ± 0.36</b>	<b>11.48 ± 0.48</b>
Freezing	91.05 ± 4.50	88.76 ± 5.44	16.15 ± 6.78
Projecting	95.78 ± 0.25	92.30 ± 0.97	11.77 ± 0.81
Schioppa et al. (2022)	97.84 ± 0.00	93.25 ± 0.00	14.22 ± 0.00
Koh & Liang (2017)	97.84 ± 0.00	93.25 ± 0.00	14.22 ± 0.00
Basu et al. (2020a)	98.23 ± 0.01	86.30 ± 0.02	21.75 ± 0.02
Retraining	99.96	99.98	9.40

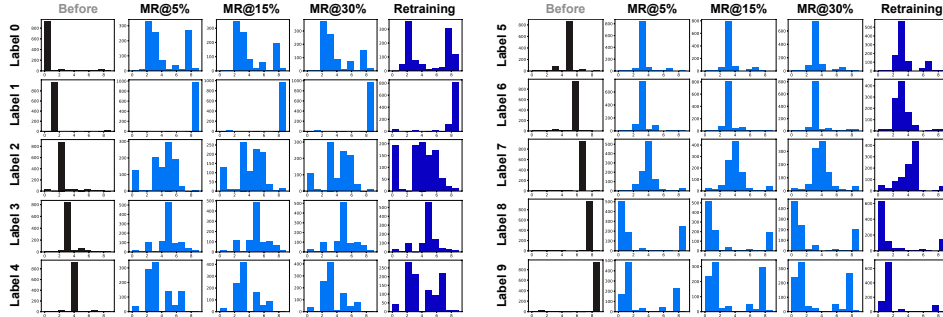


Figure 5: Inference histogram from the five models: the original model before removal, the three models updated by the GIF, and the retrained model.

**Grad-Cam visualization.** We visualized Grad-Cam results by feed-forwarding the removed and remaining images to the five models obtained by the same process as the inference histogram. The fifth and sixth convolutional layers (Conv2d) are selected for analysis because gradient outputs from earlier layers provide overly detailed outputs and those from later layers are excessively coarse. The updated models  $MR@\{5, 15, 30\}\%$  shows a similar heatmap to the **retraining** for the removed images. Interestingly, these four models tend to avoid the heatmap obtained by the model **before**. For the remaining images, the heatmap patterns from  $MR@\{5, 15, 30\}\%$  are more similar to the **before** than the **retraining**, as they mostly share the same parameters. However, all patterns show a negligible discrepancy as the five models provide correct inferences for the remaining images.

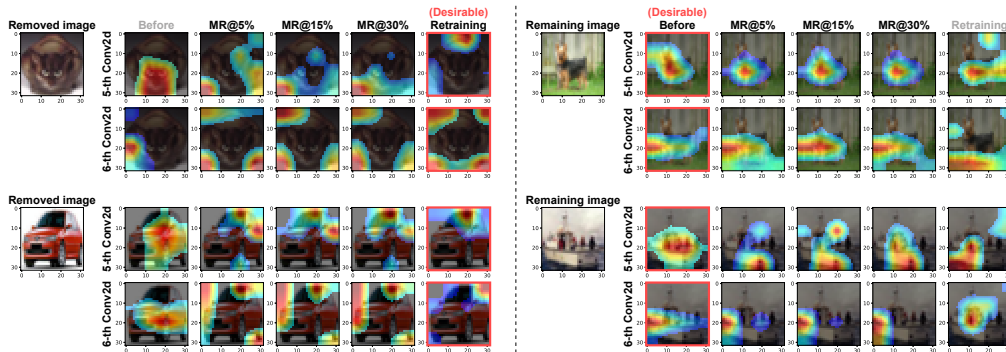


Figure 6: Grad-Cam visualization from the five models for the erased and remaining images.

## 6 Limitations, Challenges, and Future Works

**Limitations: Verification in large models.** Though the GIFs are verified to provide more accurate and reliable influence estimation than the previous works, this work does not yield results for larger models due to hardware constraints. Influence functions require substantial memory and computational overhead due to inverse Hessian operations. To date, few studies have been proposed to accelerate the computation of influence functions Kwon et al. (2024). The absence of efficient acceleration methods largely hinders the widespread adoption of influence functions.

**Challenges: How to accelerate influence functions?** Essentially, influence functions are closely related to the model fine-tuning as both require a well-trained model. Thus, low-rank adaptation or quantization might be adopted to accelerate influence computation. Moreover, the influence of data might be computed by only using the gradient without computing the Hessian, derivatives of gradients. An early attempt has been empirically made by considering the Hessian as identity Schioppa et al. (2022), but deeper analysis would be required.

Continued research will focus on enhancing the efficiency and accuracy of influence functions, as well as gaining a comprehensive understanding of the nature of network behaviors. This endeavor aims to provide us with complete accessibility to AI models.

## References

- Agarwal, N., Bullins, B., and Hazan, E. Second-order stochastic optimization for machine learning in linear time. *Journal of Machine Learning Research*, 18(116):1–40, 2017. URL <http://jmlr.org/papers/v18/16-491.html>.
- Anderson, M. ‘AI pause’ open letter stokes fear and controversy. *IEEE Spectrum*, 04 2023. URL <https://spectrum.ieee.org/ai-pause-letter-stokes-fear>.
- Barredo Arrieta, A., Díaz-Rodríguez, N., Del Ser, J., Bennetot, A., Tabik, S., Barbado, A., Garcia, S., Gil-Lopez, S., Molina, D., Benjamins, R., Chatila, R., and Herrera, F. Explainable artificial intelligence (XAI): Concepts, taxonomies, opportunities and challenges toward responsible AI. *Information Fusion*, 58:82–115, 2020. ISSN 1566-2535.
- Basu, S., You, X., and Feizi, S. On second-order group influence functions for black-box predictions. In *Proceedings of the 37th International Conference on Machine Learning, ICML’20*. JMLR.org, 2020a.
- Basu, S., You, X., and Feizi, S. On second-order group influence functions for black-box predictions. In *Proceedings of the 37th International Conference on Machine Learning*, pp. 715–724, July 2020b.
- Basu, S., Pope, P. E., and Feizi, S. Influence functions in deep learning are fragile. In *In Proceedings of the 9th International Conference on Learning Representations*, 2021.
- Bau, D., Zhu, J.-Y., Strobelt, H., Lapedriza, A., Zhou, B., and Torralba, A. Understanding the role of individual units in a deep neural network. *Proceedings of the National Academy of Sciences*, 117(48):30071–30078, 2020. doi: 10.1073/pnas.1907375117. URL <https://www.pnas.org/doi/abs/10.1073/pnas.1907375117>.
- Ben-Israel, A. and Greville, T. N. *Generalized inverses: theory and applications*, volume 15. Springer Science & Business Media, 2003.
- Bertsekas, D. *Nonlinear Programming*, volume 4. Athena Scientific, 2016.
- Cohen, G. and Giryes, R. Membership inference attack using self influence functions, 2022.
- Emerson, R. W. *Self-Reliance*, pp. 79–116. Project Gutenberg, 1841.
- Epifano, J. R., Ramachandran, R. P., Masino, A. J., and Rasool, G. Revisiting the fragility of influence functions. *Neural Networks*, 162:581–588, 2023. ISSN 0893-6080. doi: <https://doi.org/10.1016/j.neunet.2023.03.029>. URL <https://www.sciencedirect.com/science/article/pii/S0893608023001648>.
- Frankle, J. and Carbin, M. The lottery ticket hypothesis: Finding sparse, trainable neural networks. In *In Proceedings of the 7th International Conference on Learning Representations*, 2019. URL <https://openreview.net/forum?id=rJl-b3RcF7>.
- Gong, X., Yuan, D., and Bao, W. Partial label learning via label influence function. In Chaudhuri, K., Jegelka, S., Song, L., Szepesvari, C., Niu, G., and Sabato, S. (eds.), *Proceedings of the 39th International Conference on Machine Learning*, volume 162 of *Proceedings of Machine Learning Research*, pp. 7665–7678. PMLR, 17–23 Jul 2022. URL <https://proceedings.mlr.press/v162/gong22c.html>.
- Grosse, R., Bae, J., Anil, C., Elhage, N., Tamkin, A., Tajdini, A., Steiner, B., Li, D., Durmus, E., Perez, E., Hubinger, E., Lukošiūtė, K., Nguyen, K., Joseph, N., McCandlish, S., Kaplan, J., and Bowman, S. R. Studying large language model generalization with influence functions, 2023.
- Guo, H., Rajani, N., Hase, P., Bansal, M., and Xiong, C. FastIF: Scalable influence functions for efficient model interpretation and debugging. In *Proceedings of the 2021 Conference on Empirical Methods in Natural Language Processing*, pp. 10333–10350, November 2021.
- Hampel, F. R. The influence curve and its role in robust estimation. *Journal of the American Statistical Association*, 69(346):383–393, 1974.

- Hu, H., Peng, R., Tai, Y., and Tang, C. Network trimming: A data-driven neuron pruning approach towards efficient deep architectures. *CoRR*, abs/1607.03250, 2016. URL <http://arxiv.org/abs/1607.03250>.
- Jain, S., Manjunatha, V., Wallace, B., and Nenkova, A. Influence functions for sequence tagging models. In *Proceedings of the 2022 Conference on Empirical Methods in Natural Language Processing*, pp. 824–839, December 2022. URL <https://aclanthology.org/2022.findings-emnlp.58>.
- Koh, P. W. and Liang, P. Understanding black-box predictions via influence functions. In *Proceedings of the 34th International Conference on Machine Learning*, pp. 1885–1894, 2017.
- Koh, P. W., Ang, K.-S., Teo, H. H. K., and Liang, P. On the accuracy of influence functions for measuring group effects. In *Proceedings of the 33rd International Conference on Neural Information Processing Systems*, pp. 5254–5264, December 2019.
- Koh, P. W., Steinhardt, J., and Liang, P. Stronger data poisoning attacks break data sanitization defenses. *Machine Learning*, 111(1):1–47, jan 2022. ISSN 0885-6125. doi: 10.1007/s10994-021-06119-y. URL <https://doi.org/10.1007/s10994-021-06119-y>.
- Kong, S., Shen, Y., and Huang, L. Resolving training biases via influence-based data relabeling. In *The 10th International Conference on Learning Representations, 2022*. URL <https://openreview.net/forum?id=EskfH0bwNVn>.
- Kwon, Y., Wu, E., Wu, K., and Zou, J. Datainf: Efficiently estimating data influence in loRA-tuned LLMs and diffusion models. In *The 12th International Conference on Learning Representations, 2024*. URL <https://openreview.net/forum?id=9m02ib92Wz>.
- Lanczos, C. An iteration method for the solution of the eigenvalue problem of linear differential and integral operators. *Journal of research of the National Bureau of Standards*, 45:255–282, 1950. URL <https://api.semanticscholar.org/CorpusID:478182>.
- Lee, D., Park, H., Pham, T., and Yoo, C. D. Learning augmentation network via influence functions. In *Proceedings of 2020 IEEE/CVF Conference on Computer Vision and Pattern Recognition*, June 2020.
- Lee, N., Ajanthan, T., and Torr, P. H. Snip: Single-shot network pruning based on connection sensitivity. In *Proceedings of the 7th International Conference on Learning Representations*, 2019.
- Olah, C., Satyanarayan, A., Johnson, I., Carter, S., Schubert, L., Ye, K., and Mordvintsev, A. The building blocks of interpretability. *Distill*, 2018. doi: 10.23915/distill.00010. <https://distill.pub/2018/building-blocks>.
- Pearlmutter, B. A. Fast Exact Multiplication by the Hessian. *Neural Computation*, 6(1):147–160, 01 1994. ISSN 0899-7667. doi: 10.1162/neco.1994.6.1.147.
- Penny, W. D., Friston, K. J., Ashburner, J. T., Kiebel, S. J., and Nichols, T. E. *Statistical Parametric Mapping: the Analysis of Functional Brain Images*. Academic Press, 2011.
- Schioppa, A., Zablotskaia, P., Vilar, D., and Sokolov, A. Scaling up influence functions. In *Proceedings of the AAAI Conference on Artificial Intelligence*, volume 36, pp. 8179–8186, 2022.
- Selvaraju, R. R., Cogswell, M., Das, A., Vedantam, R., Parikh, D., and Batra, D. Grad-cam: Visual explanations from deep networks via gradient-based localization. In *Proceedings of 2017 IEEE International Conference on Computer Vision*, pp. 618–626, 2017. doi: 10.1109/ICCV.2017.74.
- Stewart, G. W. *Matrix algorithms*. Society for Industrial and Applied Mathematics, 2001.
- Transtrum, M. K., Machta, B. B., and Sethna, J. P. Geometry of nonlinear least squares with applications to sloppy models and optimization. *Phys. Rev. E*, 83:036701, Mar 2011. doi: 10.1103/PhysRevE.83.036701. URL <https://link.aps.org/doi/10.1103/PhysRevE.83.036701>.

- Wang, C., Zhang, G., and Grosse, R. Picking winning tickets before training by preserving gradient flow. In *In Proceedings of the 8th International Conference on Learning Representations*, 2020. URL <https://openreview.net/forum?id=SkgsACVKPH>.
- Wu, G., Hashemi, M., and Srinivasa, C. PUMA: Performance unchanged model augmentation for training data removal. *Proceedings of the AAAI Conference on Artificial Intelligence*, 36(8): 8675–8682, Jun. 2022. doi: 10.1609/aaai.v36i8.20846. URL <https://ojs.aaai.org/index.php/AAAI/article/view/20846>.
- Wu, J., Yang, Y., Qian, Y., Sui, Y., Wang, X., and He, X. Gif: A general graph unlearning strategy via influence function. In *Proceedings of the ACM Web Conference 2023, WWW '23*, pp. 651–661, New York, NY, USA, 2023. Association for Computing Machinery. ISBN 9781450394161. doi: 10.1145/3543507.3583521. URL <https://doi.org/10.1145/3543507.3583521>.
- Yang, S., Xie, Z., Peng, H., Xu, M., Sun, M., and Li, P. Dataset pruning: Reducing training data by examining generalization influence. In *The Eleventh International Conference on Learning Representations*, 2023. URL <https://openreview.net/forum?id=4wZiAXD29TQ>.
- Ye, J., Gao, J., Wu, Z., Feng, J., Yu, T., and Kong, L. ProGen: Progressive zero-shot dataset generation via in-context feedback. In *Proceedings of the 2022 Conference on Empirical Methods in Natural Language Processing*, pp. 3671–3683, December 2022. URL <https://aclanthology.org/2022.findings-emnlp.269>.
- Yoon, Y., Nam, J., Yun, H., Lee, J., Kim, D., and Ok, J. Few-shot unlearning by model inversion, 2023.

## A Studies on the regularization weight for the LiSSA iteration

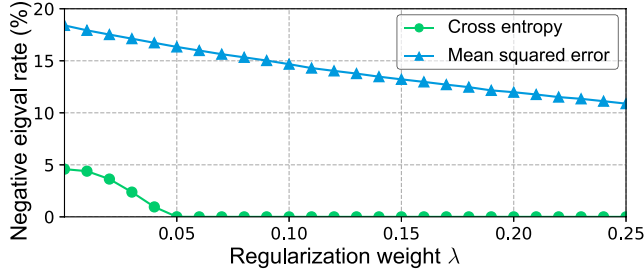


Figure 7: Percentage of negative eigenvalues vs.  $L_2$  regularization weight  $\lambda$  for the MNIST classification task on the fully-connected network.

Figure 7 shows the percentage of negative eigenvalues among the top 500 eigenvalues with the largest absolute values in the Hessian matrix, obtained from the Lanczos algorithm Lanczos (1950). The negative eigenvalue rate for the cross-entropy implies that the Hessian matrix is positive semi-definite for large enough  $\lambda$ . However, there is no way to pre-determine the proper  $\lambda$  for a given network. Moreover, such  $\lambda$  may exist outside of the viable range as in the case of the mean squared error.

## B Detailed Explanations on toy example

Figure 2 illustrates how the first two weights of the linear regression model change when the 200 heterogeneous data points are removed<sup>5</sup>. The other three weights and the bias are supposed to be fixed to observe the effect on the partial influence of the data removal. The weights are properly updated close to the optimum by the GIF, but none of the cases are for the Freezing and Projecting.

These misdirected updates are mathematically inevitable in the Freezing and Projecting schemes. The derivative of Freezing can be represented as

$$0 \approx \epsilon \nabla_{\theta_J} \ell(z, \hat{\theta}) + \begin{bmatrix} \mathbf{H}_{J \times J} & \mathbf{0} \\ \mathbf{0} & \mathbf{0} \end{bmatrix} \begin{bmatrix} \Delta_\epsilon \\ \mathbf{0} \end{bmatrix}, \quad (10)$$

where  $\mathbf{H}_{J \times J} \in \mathbb{R}^{k \times k}$ . The matrix  $\mathbf{H}_{J \times J}$  is essentially  $\mathbf{H}_J$  with all rows where the index  $j > k$  are eliminated. As a consequence, the loss of information within the gradients and Hessians leads to misdirected updates.

The Projecting generates the wrong update direction because matrix  $\mathbf{H}_{\hat{\theta}}$  is non-orthogonal. We note that  $\mathbf{H}_J (\mathbf{H}_J^T \mathbf{H}_J)^{-1} \mathbf{H}_J^T$  is a projection matrix, then  $\mathcal{I}(z, \hat{\theta}_J | \hat{\theta})$  can be considered as projection coefficients. Then, the Projecting attempts to use the coefficients from another space (column space of  $\mathbf{H}$ ) to properly project  $\nabla \ell(z, \hat{\theta})$  onto the column space of  $\mathbf{H}_J$ . This only works when  $\mathbf{H}$  is orthogonal, which is rarely the case.

## C Derivation of Generalized Influence Function

Let  $\hat{\theta}(\epsilon, \mathbf{w})$  be a minimizer of  $\mathcal{L}(\theta) + \epsilon \sum_{i=1}^m w_i \ell(z_i, \theta)$ . Then, the first-order optimality condition on the empirical risk gives

$$0 \approx \nabla \mathcal{L}(\hat{\theta}(\epsilon, \mathbf{w})) + \epsilon \sum_{i=1}^m w_i \nabla \ell(z_i, \hat{\theta}(\epsilon, \mathbf{w})). \quad (11)$$

<sup>5</sup>1000 data points are artificially manipulated by a linear mapping from  $\mathbb{R}^5$  to  $\mathbb{R}$ . 20% of data points are given heterogeneous properties by amplifying and flipping their sizes and signs, respectively.

The first-order Taylor expansion of (11) anchored on  $\hat{\boldsymbol{\theta}} = \operatorname{argmin}_{\boldsymbol{\theta} \in \Theta} \mathcal{L}(\boldsymbol{\theta})$ , is

$$0 \approx \nabla \mathcal{L}(\hat{\boldsymbol{\theta}}) + \nabla^2 \mathcal{L}(\hat{\boldsymbol{\theta}}) \left( \begin{bmatrix} \hat{\boldsymbol{\theta}}_J(\epsilon, \mathbf{w}) \\ \hat{\boldsymbol{\theta}}_{-J} \end{bmatrix} - \begin{bmatrix} \hat{\boldsymbol{\theta}}_J \\ \hat{\boldsymbol{\theta}}_{-J} \end{bmatrix} \right) + \epsilon \sum_{i=1}^m w_i \nabla \ell(z_i, \hat{\boldsymbol{\theta}}) + \epsilon \sum_{i=1}^m w_i \nabla^2 \ell(z_i, \hat{\boldsymbol{\theta}}) \left( \begin{bmatrix} \hat{\boldsymbol{\theta}}_J(\epsilon, \mathbf{w}) \\ \hat{\boldsymbol{\theta}}_{-J} \end{bmatrix} - \begin{bmatrix} \hat{\boldsymbol{\theta}}_J \\ \hat{\boldsymbol{\theta}}_{-J} \end{bmatrix} \right) \quad (12)$$

$$= \epsilon \sum_{i=1}^m w_i \nabla \ell(z_i, \hat{\boldsymbol{\theta}}) + \sum_{i=1}^m (1 + \epsilon w_i) \nabla^2 \ell(z_i, \hat{\boldsymbol{\theta}}) \Delta_\epsilon \quad (13)$$

$$= \epsilon \sum_{i=1}^m w_i \nabla \ell(z_i, \hat{\boldsymbol{\theta}}) + \mathbf{H}_J \Delta_\epsilon. \quad (14)$$

We apply the first-order optimality condition  $\nabla \mathcal{L}(\hat{\boldsymbol{\theta}}) \approx 0$  as  $\hat{\boldsymbol{\theta}}$  to (12) as  $\nabla \mathcal{L}(\hat{\boldsymbol{\theta}})$  is a minimizer of  $\mathcal{L}(\cdot)$ .

The above equation is an overdetermined linear problem, which contains no solution. Instead, we find  $\Delta_\epsilon$  that minimizes the mean squared error, which can be defined as

$$\Delta_\epsilon = \operatorname{argmin}_{\Delta \in \mathbb{R}^k} \|f(\Delta)\|_2^2, \quad (15)$$

where  $f(\Delta) = \epsilon \sum_{i=1}^m w_i \nabla \ell(z_i, \hat{\boldsymbol{\theta}}) + \mathbf{H}_J \Delta$ . Then, the solution is provided as (6).

## D Derivation of Modified LiSSA Iteration

We can derive the series (8) by simply applying the Neuman series to the GIF.

**Theorem D.1** (Neuman series). *If  $\rho(\mathbf{A}) < 1$  for a square matrix  $\mathbf{A}$ , the series  $\mathbf{A}_k = \sum_{i=0}^k (\mathbf{I} - \mathbf{A})^i$  converges to  $\mathbf{A}^{-1}$  as  $k \rightarrow \infty$ . That is,  $\mathbf{A}^{-1} = \sum_{i=0}^{\infty} (\mathbf{I} - \mathbf{A})^i$ .*

Also,  $\mathbf{A}_k$  can be incrementally defined as

$$\mathbf{A}_k = \mathbf{I} + \sum_{i=1}^k (\mathbf{I} - \mathbf{A})^i \quad (16)$$

$$= \mathbf{I} + (\mathbf{I} - \mathbf{A}) \mathbf{A}_{k-1}. \quad (17)$$

Then, putting  $\mathbf{A} = \mathbf{H}_J^\top \mathbf{H}_J$  and multiplying  $\mathcal{I}_0 = \mathbf{H}_J^\top \left[ \sum_{i=1}^m w_i \nabla \ell(z_i, \hat{\boldsymbol{\theta}}) \right]$  to the both side of (17) result in the series (8).

## E Proof of Proposition 3.1

We first show the scale-invariance of the GIF. For  $M > 0$ , we define the downscaled loss function and empirical risk as  $\frac{1}{M} \ell(z, \hat{\boldsymbol{\theta}})$  and  $\frac{1}{M} \mathcal{L}(\hat{\boldsymbol{\theta}})$ . For a given index set  $J$ , the GIF of the newly defined empirical risk is represented as

$$\left( \frac{1}{M} \mathbf{H}_J^\top \frac{1}{M} \mathbf{H}_J \right)^{-1} \frac{1}{M} \mathbf{H}_J^\top \frac{1}{M} \nabla \ell(z, \hat{\boldsymbol{\theta}}) \quad (18)$$

$$= (\mathbf{H}_J^\top \mathbf{H}_J)^{-1} \mathbf{H}_J^\top \nabla \ell(z, \hat{\boldsymbol{\theta}}) = \mathcal{I}(z, \hat{\boldsymbol{\theta}}_J | \hat{\boldsymbol{\theta}}). \quad (19)$$

Thus, the influence function is scale-invariant on the empirical risk.

The series (8) for the  $\frac{1}{M}$ -scaled loss converges only if the spectral radius of  $\mathbf{I} - \frac{1}{M^2} \mathbf{H}_J^\top \mathbf{H}_J$  is less than 1. We prove the second argument in Prop. 3.1 by showing that there exists a constant  $M$ , which makes matrix  $\mathbf{I} - \frac{1}{M^2} \mathbf{H}_J^\top \mathbf{H}_J$  positive definite with a spectral radius less than 1.

Let constant  $M = (\rho(\mathbf{H}_J^\top \mathbf{H}_J) + 1)^{\frac{1}{2}}$ . Because  $\mathbf{H}_J^\top \mathbf{H}_J$  is positive definite matrix, the spectral radius of  $\frac{1}{M^2} \mathbf{H}_J^\top \mathbf{H}_J$  is

$$0 < \rho \left( \frac{1}{M^2} \mathbf{H}_J^\top \mathbf{H}_J \right) = \frac{\rho(\mathbf{H}_J^\top \mathbf{H}_J)}{\rho(\mathbf{H}_J^\top \mathbf{H}_J) + 1} < 1, \quad (20)$$

which corresponds to

$$0 < \rho \left( I - \frac{1}{M^2} \mathbf{H}_J^T \mathbf{H}_J \right) = \frac{1}{\rho(\mathbf{H}_J^T \mathbf{H}_J) + 1} < 1. \quad (21)$$

Then, the Neumann series  $\lim_{k \rightarrow \infty} \sum_{i=0}^k \left( I - \frac{1}{M^2} \mathbf{H}_J^T \mathbf{H}_J \right)^i$  converges to  $\left( \frac{1}{M^2} \mathbf{H}_J^T \mathbf{H}_J \right)^{-1}$ .

## F Pythonic Implementation of Alg. 1

Variables in the `compute_GIF(·)` are matched with Alg. 1 as follows: `total_loss` for  $\mathcal{L}(\hat{\theta})$ ; `target_loss` for  $\mathcal{L}_w(\hat{\theta})$ ; `parser` for the selection criterion; and `parameter_indices` for the parameter set  $J$ . The `parser` internally implements the hook function in pytorch, to generate the network indices during the feed-forward (or back-propagation) stage.

Function `_GIF(·)` implements the series (8). In real implementations, computing  $\mathcal{I}_{k-1} - \mathbf{H}_J^T \mathbf{H}_J \mathcal{I}_{k-1}$  is more efficient than computing  $(I - \mathbf{H}_J^T \mathbf{H}_J) \mathcal{I}_{k-1}$ , as in lines 21-24. The hessian-vector products are applied twice to compute  $\mathbf{H}_J^T \mathbf{H}_J \mathcal{I}_{k-1}$ . One can additionally divide the two losses with some number if the series does not converge. Function `hvp` and `grad` computes the hessian-vector product; and the gradient of a given loss, respectively.

```

1  def compute_GIF(net, total_data, target_data):
2      total_loss = criterion(net, total_data)
3      parser = selection(net, num_param)
4      target_loss = criterion(net, target_data)
5      parameter_indices = parser.get_parameter_indices()
6
7      return _GIF(net, total_loss, target_loss, parameter_indices)
8
9  def _GIF(net, total_loss, target_loss, parameter_indices):
10     # I_0 in Eq. (12).
11     v = grad(net, target_loss)
12     GIF_0 = hvp(net, total_loss, v)[parameter_indices]
13
14     # Repeat until the series (12) converges.
15     while l2_norm(GIF_new - GIF_old) > tol:
16         GIF_old = GIF_new
17         GIF_new = GIF_0 + GIF_old \
18             - hvp(net, total_loss, hvp(net, total_loss, GIF_old)
19               [parameter_indices])
20     return GIF

```

Listing 1: Pythonic pseudo-code of the GIF.

## G Experimental Details for Reproduction

All experiments are conducted on the Linux workstation with AMD Ryzen™7 5800X 8-Core Processor CPU @ 3.70GHz and one NVIDIA Geforce RTX 3080Ti. Our implementation code to reproduce the results is available at <https://github.com/hslyu/dbspf>.

### G.1 Network Preparation

**VGG-11 with CIFAR-10 dataset** We adopted the same setting as ResNet-18, except for the following differences. The CIFAR-10 dataset is normalized as  $\mu = (0.4914, 0.4822, 0.4465)$  and  $\sigma = (0.2023, 0.1994, 0.2010)$ . We adopt a cosine annealing learning rate scheduler with a maximum iteration of 200. After training, the test accuracy is 91.50%.

**Custom CNN with BD MNIST dataset** We used the same configurations for Table. 2, except for the scheduler and MNIST data preparation. 30% of data is sampled by using `numpy.choice(·)` method with seed 1. The 30% of data, so-called BD data, is implanted check-pattern array that alters 0 and 16. To prevent overflow of MNIST data formatted by `uint8`, we clipped the implanted image

array elements into [0, 255]. The model is trained for 20 epochs, with the learning rate scheduled by a step scheduler that reduces the learning rate by a factor of 0.1 at the 10th and 15th epochs. We use two CNNs: one CNN is trained with BD data and BD label, and the other is trained with BD data and original label. After training, the test accuracies of the two models are 98.96% and 98.98%, respectively.

## G.2 Data Sampling

We sample the dataset twice to compute two losses; one for hessian  $\mathbf{H}_J$  and the other for gradient  $\sum_{i=1}^m w_i \nabla \ell(z_i, \hat{\theta})$ . The data sampling approach draws inspiration from second-order Hessian computation (Agarwal et al., 2017) and is in line with the research on the acceleration of influence functions (Guo et al., 2021).

## G.3 Differences Between Theoretic and Empirical Update Strategies

Influence functions measure infinitesimal parameter changes, so influence functions need to be extrapolated to estimate actual changes in the model. When the data  $z$  is removed from the model, variable  $\epsilon$  should be configured as  $\epsilon = -\frac{1}{m}$  in the  $\epsilon$ -upweighted empirical risk minimization problem  $\hat{\theta}(\epsilon, z) = \operatorname{argmin}_{\theta \in \Theta} \frac{1}{m} \sum_{i=1}^m \ell(z_i, \theta) + \epsilon \ell(z, \theta)$ . Then, from Eq. (2), the model changes  $\Delta_\epsilon$  can be computed as  $\Delta_\epsilon \approx \mathbf{H}^{-1} \nabla \ell(z, \hat{\theta}) \epsilon = \mathcal{I}(z, \hat{\theta}) \epsilon$  (Koh & Liang, 2017).

When measuring the group influence, the  $\epsilon$ -upweighted empirical risk minimization problem is configured as  $\hat{\theta}(\epsilon, \mathbf{w}) = \operatorname{argmin}_{\theta \in \Theta} \frac{1}{m} \sum_{i=1}^m \ell(z_i, \theta) + \epsilon \frac{1}{\|\mathbf{w}\|_1} \sum_{i=1}^m w_i \ell(z, \theta)$ . Then, variable  $\epsilon$  needs to be set as  $\epsilon = -\frac{\|\mathbf{w}\|_1}{m}$  to approximate the model changes in the group data removal scenario.

These theoretical  $\epsilon$  settings are known to underestimate the actual changes in the real implementations (Koh et al., 2019). Such properties are coherently observed in our implementation, making it challenging to determine the appropriate  $\epsilon$  that most accurately estimates the behavior of the retrained model.

We empirically determine the update weight  $\epsilon$  rather than using the theoretical value for the above reason. We first normalize the influence function and update the network with the update rate  $\gamma$ , which can be represented as

$$\theta_J \leftarrow \theta_J + \gamma \frac{\mathcal{I}(z, \hat{\theta}_J | \hat{\theta})}{\|\mathcal{I}(z, \hat{\theta}_J | \hat{\theta})\|_2} \quad (22)$$

with initial  $\theta_J = \hat{\theta}_J$ . Then, we update the model repetitively with  $\gamma = 0.03$  until we get the best  $F_1$  score.